Nano LIFE
Vol. 1, Nos. 3 & 4 (2010) 251–261

DOI: 10.1142/S1793984410000237

PHOSPHOLIPID ASSEMBLY ON SUPERPARAMAGNETIC NANOPARTICLES FOR THERMORESPONSIVE DRUG DELIVERY APPLICATIONS

CHRISTOPHER HUTH*, DONGLU SHI†,‡,**, FENG WANG*,
DONALD CARRAHAR*, JIE LIAN§, FENGYUAN LU§, JIAMING ZHANG¶,
RODNEY C. EWING¶ and GIOVANNI M. PAULETTI‖

*School of Energy, Environmental
Biological and Medical Engineering, University of Cincinnati
Cincinnati, Ohio 45221, USA

†The Institute for Advanced Materials and Nano Biomedicine, Tongji University
Shanghai 200092, P. R. China

‡School of Electronic and Computing Systems
University of Cincinnati, 493 Rhodes Hall, Cincinnati
OH 45221-0012, USA

§Department of Mechanical
Aerospace and Nuclear Engineering, Rensselaer Polytechnic Institute
Troy, New York 12180, USA

¶Departments of Geological Sciences
Nuclear Engineering and Radiological Sciences
and Materials Science and Engineering
University of Michigan, Ann Arbor, Michigan 48109, USA

‖James L. Winkle College of Pharmacy
University of Cincinnati, Cincinnati, Ohio 45267, USA
**shid@ucmail.uc.edu

Received 4 March 2011
Accepted 8 April 2011

Thermoresponsive nanocomposites were prepared by immobilizing a 2–3 nm thick phospholipid layer on the surface of superparamagnetic Fe_3O_4 nanoparticles via high-affinity avidin/biotin interactions. Morphological and physicochemical surface properties were assessed using transmission electron microscopy, confocal laser scanning microscopy, differential scanning calorimetry, and attenuated total reflectance Fourier transform infrared spectroscopy. The zeta potential of Fe_3O_4 colloids in phosphate buffered saline (PBS) decreased from −23.6 to −5.0 mV as a consequence of phospholipid immobilization. Nevertheless, heating properties of these superparamagnetic nanoparticles within an alternating magnetic field were not significantly affected. Hyperthermia-relevant temperatures $> 40°C$ were achieved within 10–15 min using a 7-mT magnetic field alternating at a frequency of 1 MHz. Loading of the surface-associated phospholipid layer with the hydrophobic dye dansylcadaverine was accomplished at an efficiency of 479 ng/mg Fe_3O_4. Release of this drug surrogate was

temperature-dependent, resulting in a 2.5-fold greater release rate when nanoparticles were exposed to a temperature above the experimentally determined melting temperature of 39.7°C. These data underline the feasibility of preparing novel, stimulus-induced drug delivery systems where payload release from a colloid-immobilized phospholipid assembly is triggered by hyperthermia.

Keywords: Magnetic nanoparticles; thermoresponsive materials; drug delivery; hyperthermia; cancer therapy.

1. Introduction

Controlled drug delivery systems have evolved from conventional formulations designed to maintain predefined pharmacokinetic drug profiles over prolonged periods of time to more responsive drug delivery systems engineered with stimulus-induced release mechanisms. Among those "smart" drug delivery technologies, open-loop systems constitute formulations whereby dissociation of a therapeutic moiety from its carrier is regulated externally, most frequently by physical stimuli such as light, ultrasound, or magnetic fields.[1–6]

Stimulus-controlled drug delivery systems are predicted to particularly benefit patients diagnosed with diseases that are caused by oscillating pathophysiology, including bronchial asthma, arthritis, peptic ulcer, and diabetes[7,8] In addition, these systems are expected to improve management of disease states dominated by distinct, local occurrences such as inflammation and cancer. Conventional drug delivery strategies generally rely on passive drug distribution that achieves therapeutically effective concentrations at the desired site of action. Using cancer chemotherapy as an example, highly potent cytotoxic agents are distributed throughout the body via the blood circulation systems aimed at destroying tumor cells. Nonselective and uncontrolled biodistribution, however, leads to undesired killing of normal cells with high proliferation rates. These "off-target" effects are responsible for drug-induced nausea, vomiting, diarrhea, hair loss, and bone marrow suppression.[9] Stimulus-triggered release of anticancer agents in close proximity to a tumor mass is anticipated to limit these undesired side effects and effectively improve quality of life of cancer patients.

The design of bioresponsive matrices that facilitate stimulus-activated drug delivery critically depends on adequate sensing functionalities incorporated within the carrier. As a consequence, drug release can be effectively controlled via a wireless, externally applied "on-off" switch to meet spatial and/or temporal requirements of therapeutic interventions. For many years, materials that change properties in response to temperature were explored for fabrication of stimulus-induced drug delivery systems. Biocompatible analogs of poly(*N*-substituted acrylamide), poly(ethylene glycol), and phospholipids have emerged as leading polymers since they undergo reversible volume or sol-gel phase transition within 36−45°C, which corresponds to a temperature range spanning physiological environment to mild hyperthermia.[10–13] Clinical hyperthermia, in particular, has gained attraction for drug delivery applications in cancer patients after several clinical studies demonstrated that heating of tumor tissue up to 45°C significantly enhances efficacy of chemotherapy and radiation.[13]

Magnetic nanocarriers, including nanoparticles composed of superparamagnetic materials such as Fe_3O_4 or liposomes/polymeric micelles containing encapsulated magnetic nanoparticles, are presently evaluated for a diverse array of drug delivery, biomedical diagnostic, and analytical applications.[12–14] Appropriately tailored magnetic properties facilitate accumulation in a target tissue guided by a strong, external magnetic field (i.e., magnetic drug targeting).[15,16] Furthermore, exposure of magnetic nanocarriers to an alternating magnetic field induces local heating that effectively translates into therapeutic hyperthermia.[13,17,18] Combination of these magnetic nanocarriers with thermosensitive polymers have resulted in bioresponsive nanocomposites suitable for stimulus-induced drug delivery applications. To date, coprecipitation of superparamagnetic Fe_3O_4 in the presence of thermosensitive polymers is an accepted standard for fabrication of bioresponsive nanocomposites[13,19] Using this methodology, processing variables such as Fe_3O_4/polymer ratio, solvent system, and stirring rate critically affect Fe_3O_4 encapsulation efficiency and, consequently, the overall magnetic moment of the nanocomposite, particle size distribution, and thermoresponsive properties. Considering the added requirement for incorporation of a therapeutic payload into these

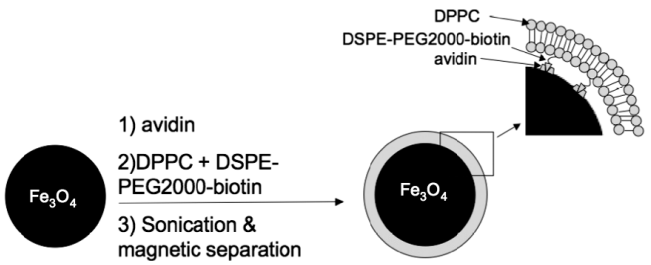

Fig. 1. Schematic overview of layered phospholipid assembly on superparamagnetic nanoparticles. Phospholipid bilayer is immobilized on the surface of avidin-coated Fe_3O_4 nanoparticles using high-affinity binding interactions with DSPE-PEG2000-biotin anchors embedded at 5% (w/w) within the DPPC layer.

bioresponsive systems, it becomes evident that alternative fabrication methods need to be explored to reproducibly prepare thermoresponsive magnetic nanocarriers suitable for drug delivery applications.

In this study, we explored a unique phospholipid assembly immobilized as bilayer on superparamagnetic Fe_3O_4 nanoparticles via high-affinity avidin−biotin binding interactions (Fig. 1). To investigate loading efficiency and temperature-dependent release of a carrier-associated payload, the lipophilic dye dansylcadaverine was incorporated into the phospholipid bilayer as drug surrogate. Materials properties of the thermoresponsive nanoparticles were assessed by differential scanning calorimetry (DSC) and attenuated total reflectance Fourier transform infrared spectroscopy (ATR-FTIR). Confocal laser scanning microscopy (CLSM) and transmission electron microscopy (TEM) were used to visualize these novel nanocomposites. Zeta potential was determined by dynamic laser light scattering (DLS). Magnetically induced hyperthermia was monitored using a field strength of 7-mT at a frequency of 1 MHz. Payload incorporation efficiency and temperature-dependent release was quantified by fluorescence spectroscopy.

2. Materials and Methods

2.1. *Materials*

1, 2-Dipalmitoyl-*sn*-glycero-3-phosphocholine (DPPC) and the ammonium salt of 1, 2-distearoyl-*sn*-glycero-3-phosphoethanolamine-*N*-[biotinyl(polyethylene glycol)-2000] (DSPE-PEG2000-biotin) were purchased from Avanti Polar Lipids Inc. (Alabaster, AL, USA). The triethylamine salt of 1,2-dipalmitoyl-*sn*-glycero-3-phosphoethanolamine-*N*-(7-nitro-2-1, 3-benzoxadiazol-4-yl) (NBD-DSPE, EX = 445 nm and EM = 507 nm) was obtained from NOF America (White Plains, NY, USA). Avidin was purchased from ProSPEC (East Brunswick, NJ), and dansylcadaverine was supplied by Sigma Aldrich (St. Louis, MO, USA). Fe_3O_4 nanoparticles (100 nm average diameter, FE120904-M6-2) were purchased from Nanophase, Inc. (Romeoville, IL, USA). Superparamagnetic iron microbeads (5 μm diameter, # FB-104) were purchased from Bioclone, Inc. (San Diego, CA, USA).

2.2. *Phospholipid assembly on colloid surface*

Phospholipid bilayers were immobilized on the surface of superparamagnetic colloids via high-affinity avidin−biotin binding interactions using a protocol adapted from the literature.[20] Briefly, 1 mL of Fe_3O_4 nanoparticle suspension (0.24 mg/mL) were washed three times in a 1.5 mL microcentrifuge tube with phosphate buffered saline, 7.4 (PBS) followed by magnetic separation. Subsequently, nanoparticles were suspended in 1 mL of PBS supplemented with avidin (0.05 mg/mL) and incubated at 4°C for 24 h. Excess avidin was removed by three consecutive wash cycles with PBS. In a separate 1.5-mL microcentrifuge tube, 95 μL of DPPC dissolved in chloroform (1.5 mM) were combined with 5 μL of a 0.6 mM solution of DSPE-PEG2000-biotin prepared in the same solvent. Chloroform was allowed to evaporate overnight at room temperature forming a phospholipid film along the centrifuge tube wall. The avidin-coated Fe_3O_4 nanoparticle suspension was quantitatively transferred into the tube containing the dry phospholipid film. Affinity-stabilized immobilization of phospholipid bilayers on avidin-coated nanoparticles was induced at room temperature by 10 min continuous exposure to ultrasonic waves (60 Hz) followed by an additional stabilization period of 30 min. Phospholipid-modified Fe_3O_4 nanoparticles were washed three times with PBS and resuspended in PBS until further use.

To visually monitor phospholipid immobilization by CLSM, 5-μm diameter superparamagnetic microbeads were subjected to a slightly modified protocol as described above for the smaller Fe_3O_4 nanoparticles. Instead of the DPPC/DSPE-PEG2000 (95:5) composition, avidin-coated microbeads were combined with a dry fluorescent lipid film comprised of DPPC/DSPE-PEG2000-biotin/NBD-DSPE (92.5:5.0:2.5).

2.3. *Differential scanning calorimetry*

Thermal behavior of pure DPPC and colloid-associated phospholipids was compared using a Netzsch STA 409 PC Luxx DSC (Netzsch-Gerätebau GmbH, Selb, Germany). About 1 to 2 mg of sample was sealed in aluminum pans and thermograms acquired from 25−90°C under constant nitrogen purge at a heating rate of 2°C min^{-1}. Temperature calibration was performed by running empty sample and reference pan at the same heating rate of 2°C min^{-1}. An empty pan was used as a reference.

2.4. *Attenuated total reflectance Fourier transform infrared spectroscopy*

Diamond crystal ATR-FTIR spectra were recorded for pure DPPC and DPPC/DSPE-PEG2000-biotin (95:5) phospholipid bilayers immobilized on the surface of avidin-coated Fe_3O_4 nanoparticles using a Nicolet 6700 (Thermo Fisher Scientific, Waltham, MA, USA). Each spectrum was acquired from 16 scans over a wavenumber region of 4000−400 cm^{-1} at 4 mm/s (resolution: 2 cm^{-1}) followed by computerized data analysis using OMNIC (version 7.4).

2.5. *Confocal laser scanning microscopy*

A Zeiss LSM510 META inverted confocal laser scanning microscope (Carl Zeiss MicroImaging, Thornwood, NY, USA) equipped with an argon laser emitting at 488 nm to excite NBD-DSPE-doped microbeads was used for common smear microscopic examination of control and phospholipid-modified colloids dispersed in PBS. Digital images were recorded using diffusion interference contrast (i.e., brightfield) and a 530-nm longpass filter. The NBD signal was displayed in the pseudocolor green. A 40 × /1.2 C-Apochromat (oil immersion) objective was used for routine studies.

2.6. *Transmission electron microscopy*

Ultrastructural differences between control and phospholipid-modified Fe_3O_4 nanoparticles were assessed by TEM using a JEOL 2010 high-resolution transmission electron microscope (JEOL, Inc., Commerce, MI, USA) equipped with an INCA X-ray energy dispersive spectroscopy (EDS) system. Briefly, a droplet of each sample suspension in PBS was placed on a carbon-coated copper grid and dried in air. Microscopic images were acquired at an accelerating voltage of 200 keV and subsequently analyzed by EDS.

2.7. *Zeta potential*

The electrokinetic potential of control and phospholipid-modified Fe_3O_4 nanoparticles was determined by DLS using a Zetasizer Nano (Malvern Instruments, Worcestershire, UK) equipped with a 4 mW helium/neon laser ($\lambda = 633$ nm). Dilute suspensions (≤ 2 mg/mL) prepared in PBS were transferred into low-volume cuvettes and equilibrated at 25°C for 5 min before each measurement. Scattered light was detected at a fixed angle of 173°. The refractive index, absorption, and viscosity of the colloidal suspension were assumed as 1.360, 0.001, and 0.882 cP, respectively.

2.8. *Magnetically induced hyperthermia*

Time-dependent heating curves of control and phospholipid-modified Fe_3O_4 nanoparticles upon exposure to an alternating magnetic field were measured using the Euris *In Vitro* Magnetic Field Generator (Euris, Stockholm, Sweden). Briefly, 200 μL of the nanoparticle suspension (0.24 mg/mL Fe_3O_4) in PBS was transferred into a thin-wall PCR tube and repeatedly exposed for 90 s to a 7 mT magnetic field alternating at a frequency of 1 MHz. Each magnetic pulse was separated by a period of 15 s without a magnetic field to record temperature of the aqueous vehicle using a thermocouple. Temperature readings were recorded for 30 min. Each experiment was performed in triplicate and data reported as mean ± SD.

2.9. *Loading and thermoresponsive release of dansylcadaverine*

Payload capacity of phospholipid-modified Fe_3O_4 nanoparticles was estimated using dansylcadaverine as drug surrogate. To the phospholipid mixture prepared in chloroform, 10 μL of a 745 μM stock solution of this lipophilic dye in methanol was added. Following evaporation of the organic solvents, the dry lipid film contained 5% (mol/mol) dansylcadaverine. Immobilization of phospholipid bilayers on the surface of the avidin-coated,

superparamagnetic nanoparticles was induced by ultrasonication as described above. Unincorporated dansylcadaverine was removed by three consecutive wash steps with PBS followed by magnetic separation. Dansylcadaverine loading capacity expressed as ng dansylcadaverine/mg Fe_3O_4 was quantified by resuspending dye-loaded colloids in methanol. Following overnight incubation on an orbital shaker (60 Hz) at room temperature, Fe_3O_4 nanoparticles were removed by magnetic separation and dansylcadaverine quantified using the PolarSTAR Optima (BMG Laboratory, Charlotte, NC, USA) fluorescence microplate reader equipped with 355-nm excitation and 420-nm emission filters. To assess whether release of dansylcadaverine from phospholipid-modified Fe_3O_4 nanoparticles was dependent on environmental temperature, 0.2 mg of dye-containing colloids were suspended in 1 mL of PBS and incubated for 60 min at 25°C and 70°C. Fe_3O_4 nanoparticles were removed by magnetic separation, and dansylcadaverine released into the aqueous vehicle quantified by fluorescence spectroscopy. Dye loading and release experiments were each performed using at least four different preparations. Data are reported as mean ± SD.

3. Results and Discussion

3.1. *Surface-immobilized phospholipid assembly*

Deposition of thermoresponsive phospholipids on the surface of Fe_3O_4 colloids was attempted by anchoring DPPC bilayers via a biotin bridge to avidin-coated superparamagnetic nanoparticles. This methodology was shown previously to allow facile immobilization of phospholipid bilayers on spherical silica substrates using neutral, negatively, or positively charged lipid compositions.[20] Critical to this process is avidin adsorption onto the polar Fe_3O_4 surface, which is most likely facilitated by strong hydrogen bonds.[21,22] During sonication of the lipid film in the presence of the aqueous suspension of avidin-coated colloids, it is hypothesized that DPPC bilayer vesicles with exterior facing DSPE-PEG2000-biotin anchors are formed and rearrange into spherically supported bilayers on Fe_3O_4 colloids stabilized by strong avidin–biotin interactions. TEM combined with EDS was used to investigate morphology and composition of control and phospholipid-modified nanoparticles. Figure 2(a) shows the spherical magnetite structure with a diameter of about 100 nm. The surface of this colloid seems smooth without visible associations. The dominating Fe peak in the corresponding EDS spectrum [Fig. 2(c)] confirms composition. In contrast, TEM of colloids isolated after immobilization of phospholipids clearly demonstrates the presence of an amorphous layer associated with the Fe_3O_4 surface [Fig. 2(c)]. The EDS spectrum of these modified colloids includes a carbon peak around 0.2 keV and a phosphorus peak around 2 keV, which is indicative of the presence of phospholipids [Fig. 2(d)]. As compared to the Fe and Cu peaks associated with the nanoparticle and TEM grid, respectively, phospholipid signals exhibit lower strength suggesting deposition of a thin lipid layer. Experimental predictions and computational simulations estimate the thickness of a fully hydrated DPPC bilayer between 4–6 nm[23,24] From TEM images obtained with phospholipid-modified Fe_3O_4 nanoparticles [Fig. 2(c)], it appears that the surface-immobilized DPPC/DSPE-PEG2000-biotin layer is only around 2–3 nm in diameter. Most likely, limitations associated with TEM technology prevented satisfactory visualization of lipid-associated water layers.

To assess the uniformity of surface-supported phospholipid assembly the fluorescent lipid analog NBC-DSPE was incorporated into the lipid film at 2.5% (w/w) for CLSM experiments. Instead of Fe_3O_4 nanoparticles, which were too small to visualize surface properties using this technology, magnetic microbeads (∼5 μm diameter) were subjected to the same coating protocol as described above. Figure 3(a) shows a representative micrograph of a fluorescence and brightfield overlay for bare control colloids affirming absence of significant autofluorescnece. Similar images obtained for phospholipid-modified microbeads visually reveal almost complete coverage of the colloid surface with the NBD-DSPE-labeled lipid phase represented by the pseudogreen color [Figs. 3(b) and 3(c)]. Previously, Gopalakrishnan and colleagues used similar CLSM technology to demonstrate that incubation of polar silica particles with a fluorescent avidin analog achieves uniform surface coating.[20] Combined with our data obtained with a fluorescent lipid analog, these results underline successful immobilization of phospholipid bilayers on polar surfaces stabilized by high-affinity binding interactions between colloid-adsorbed avidin and lipid-associated biotin anchors. In this study, phospholipid layers were assembled on polar, avidin-coated colloid surfaces using

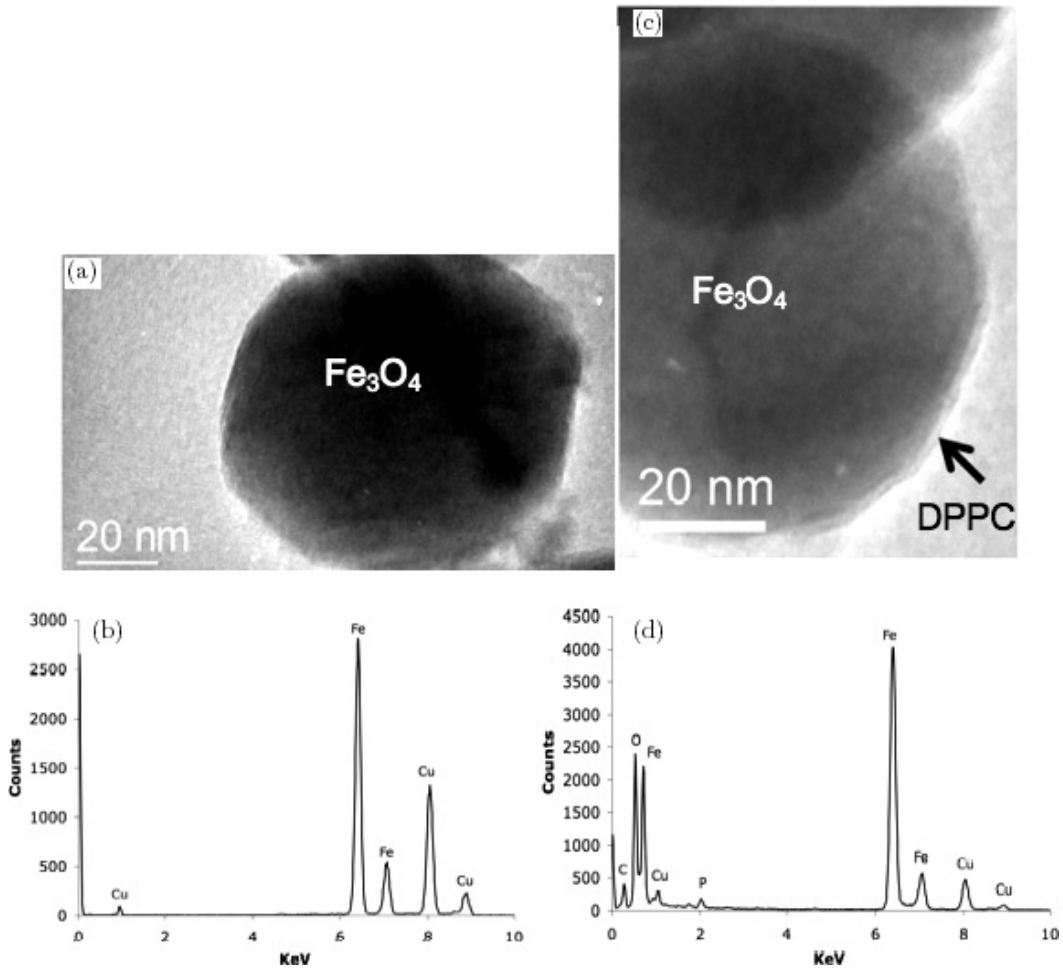

Fig. 2. TEM images and EDS spectra of control and phospholipid-modified Fe_3O_4 nanoparticles. Panels (a) and (b) show morphology and materials composition of purified Fe_3O_4 nanoparticles. Panels (c) and (d) show structure and materials properties of phospholipid-modified colloids prepared by sonication of an aqueous, avidin-coated Fe_3O_4 nanoparticle suspension with a dried DPPC/DSPE-PEG2000-biotin lipid film.

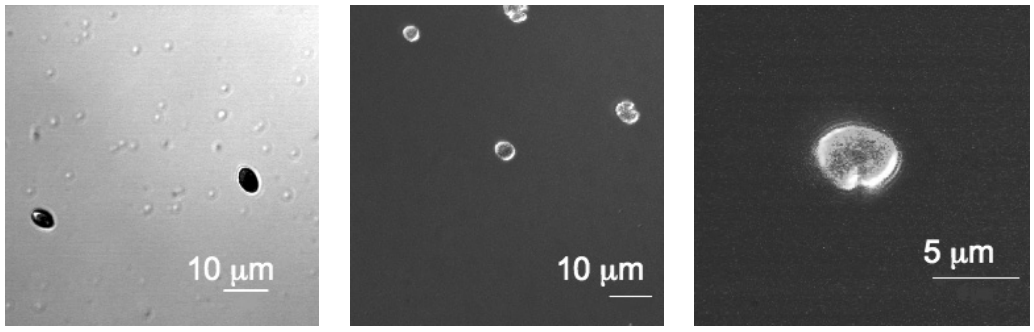

(a) (b) (c)

Fig. 3. Confocal images of phospholipid-modified microbeads. (a) Representative overlay of brightfield and fluorescence images of $\sim$5 μm control microbeads. (b) Representative overlay of brightfield and fluorescence image of microbeads following immobilization of DPPC/DSPE-PEG2000-biotin/NBC-DSPE phospholipid layer. NBD-associated fluorescence emission is displayed in the pseudocolor green. (c) Increased magnification of representative phospholipid-modified microbead.

ultrasonication dispersion of a dried lipid film in aqueous environment. Thermodynamically, immobilization of phospholipid bilayers on colloid surface is predicted to occur in parallel with undesired formation of liposome-like phospholipid vesicles. Future experiments will have to explore quantitative aspects of these competing events and assess the impact of particle size and lipid concentration on coating efficiency of the colloid surface. Intrinsic magnetic properties of Fe_3O_4 nanoparticles and microbeads used in this study successfully facilitated separation of phospholipid-modified colloids from liposome-like phospholipid vesicles.

3.2. *Surface properties of phospholipid-modified Fe_3O_4 nanoparticles*

Thermal properties of fabricated nanocomposites that control temperature-dependent release of carrier-associated payload were determined by DSC (Fig. 4). The thermogram of pure DPPC shows a broad endothermic behavior with an estimated melting temperature (T_m) of 42.0°C, which is consistent with reported literature values for the main (P'_β/L_α) phase transition.[25,26] In contrast, the gel/liquid-crystalline phase transition of the surface-immobilized phospholipid layer occurred at a peak T_m of 39.7°C. The reduced enthalpy measured for the colloid-associated lipid layer can be explained by the significant contribution of the Fe_3O_4 particle core to the sample weight. Reduction in temperature may be explained by the 5% (w/w) addition of

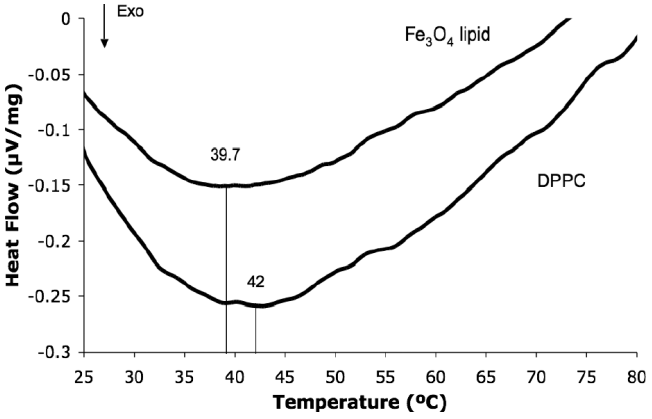

Fig. 4. DSC thermograms illustrating gel/liquid-crystalline phase transition of pure DPPC ("DPPC") and DPPC/DSPE-PEG2000-biotin (95:5) phospolipid layer immobilized on avidin-coated Fe_3O_4 nanoparticles ("Fe_3O_4 lipid").

DSPE-PEG2000-biotin to the DPPC lipid phase. Interestingly, Kastantin and co-workers were unable to detect a distinct transition temperature of DSPE-PEG2000 between 0–90°C.[27] Consequently, we hypothesize that the small shift in T_m results from increased lateral tension of surface-immobilized phospholipids that energetically favors lower melting temperatures.[28] Furthermore, greater radius of curvature due to the small size of phospholipid-supporting nanoparticles is also expected to lower T_m.[29]

ATR-FTIR was used to compare chemical features of surface-immobilized phospholipid layers to pure DPPC (Fig. 5). The most prominent features were divided into four spectral regions. Panel a shows intense IR bands around 2850 and 2915 cm^{-1} that correspond to CH_2 asymmetric and symmetric stretching modes of the acyl chains in DPPC. It is notable that the intensity of these bands is significantly reduced in colloid-associated phospholipids. As the amount of lipids deposited on Fe_3O_4 nanoparticles is presumably small, it is conceivable that FTIR was not sensitive enough to detect these stretching modes. Similarly, the ester C=O stretching band near 1735 cm^{-1} is distinct for pure DPPC but broadened from about 1730 to 1830 cm^{-1} in the colloid-associated lipid layer, with an apparent peak at 1790 cm^{-1} (Fig. 5, Panel b). In general, it is accepted that incorporation of water into DPPC layers results in broader IR bands due to formation of hydrogen bonds.[30] In the phospholipid headgroup region, the characteristic asymmetric stretching band of the PO_2^- around 1240 cm^{-1} is clearly visible in both preparations (Fig. 5, Panel c). The most prominent difference in IR spectra, however, is the dramatic increase in relative intensity of the CH_2 scissoring bands at 1466 and 1357 cm^{-1}, respectively. This behavior is consistent with changes in direction of the transient dipole vector of an adsorbed lipid molecule through electrostatic interactions.[31]

The surface charge of colloidal systems measured as zeta potential directly correlates with chemical properties of surface-associated coatings and, in addition, defines dispersion stability in aqueous or nonaqueous media. Purified control Fe_3O_4 nanoparticles exhibited a zeta potential of -23.6 ± 1.3 mV in PBS, which is consistent with previous reports for this material.[32] The dominant negative charge associated with these colloids facilitates effective repulsion of individual nanoparticles, which translates into measurable suspension stability in PBS for up to 2 h. In contrast, the zeta potential measured for

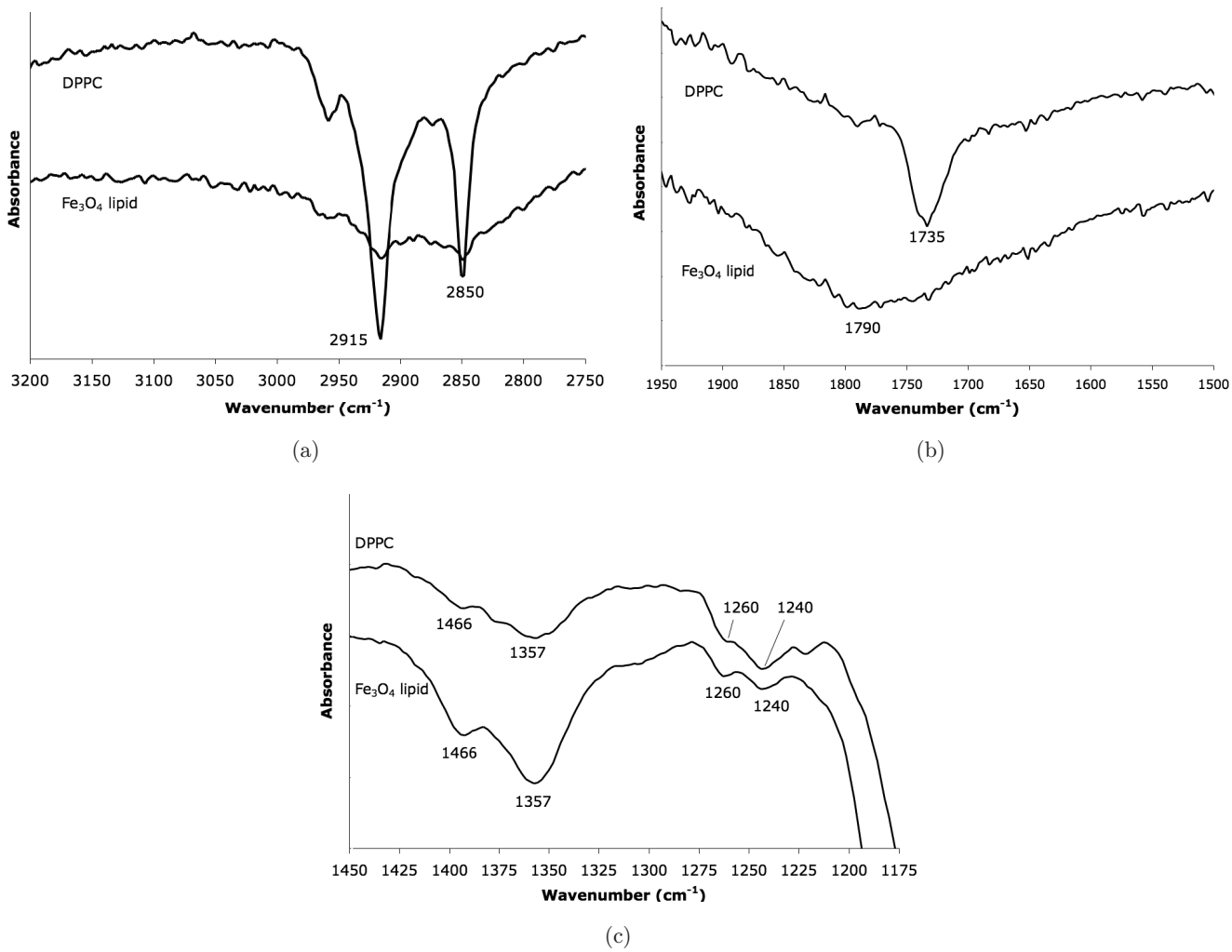

Fig. 5. ATR-FTIR absorbance spectra of pure DPPC ("DPPC") and DPPC/DSPE-PEG2000-biotin (95:5) immobilized on the surface of avidin-coated Fe_3O_4 nanoparticles ("Fe_3O_4 lipid"). Expanded regions are shown for CH_2 asymmetric and symmetric stretching of acyl chains (Panel a), C=O stretching (Panel b), and CH_2 scissoring and asymmetric PO_2^- stretching (Panel c).

phospholipid-modified Fe_3O_4 nanoparticles was only -5.0 ± 3.0 mV, which is comparable to values reported for DPPC dispersion in aqueous solutions.[33] This significant change in surface charge supports successful assembly of a phospholipid layer on these superparamagnetic nanoparticles. However, it also implies substantially decreased dispersion stability as compared to control nanoparticles, which was experimentally confirmed. Phospholipid-coated Fe_3O_4 nanoparticles begin to sediment within 5−10 min after dispersion. Nevertheless, colloids with slightly positive or negative zeta potentials demonstrate reduced adsorption capacities for serum components such as proteins and lipoproteins.[32] This may result in more consistent biodistribution pattern as compared to colloids with dramatically stronger surface charges.

3.3. *Magnetically induced hyperthermia*

Thermoresponsive release of a payload incorporated into phospholipid-modified nanoparticles depends on heating properties of these superparamagnetic colloids within an alternating magnetic field. Figure 6 compares the temperature time course of 1 mL of control and phospholipid-coated Fe_3O_4 nanoparticles suspensions prepared in PBS (0.24 mg/mL) following exposure to 7-mT magnetic field pulses alternating at a frequency of 1 MHz. After a 3-min lag time, both preparations show fairly linear increases in temperature within the first 15 min. The slope calculated for this steady state hyperthermia was 1.50 ± 0.04°C/min and 1.38 ± 0.05°C/min for bare and phospholipid-modified nanoparticles, respectively. Theoretically, heating

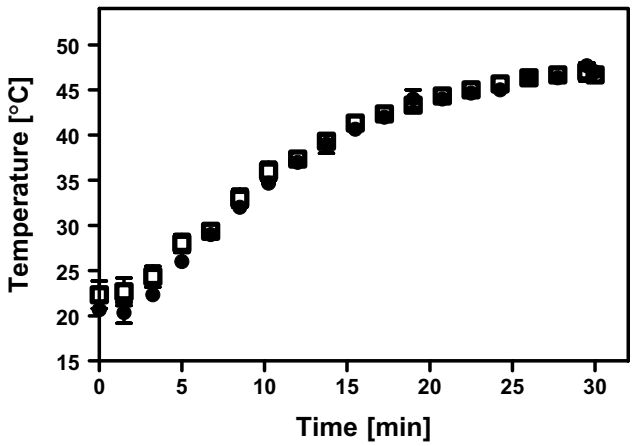

Fig. 6. Heating properties of superparamagnetic Fe_3O_4 suspensions within an alternating magnetic field. Bare control (□) and phospholipid-modified (•) Fe_3O_4 nanoparticles were suspended at 0.24 mg/mL in PBS. Temperature of suspension was monitored for 30 min while repeatedly exposed for 90 s to a 7-mT magnetic field alternating at a frequency of 1 MHz. Data are shown as mean ± SD ($n = 3$).

effects of magnetic nanoparticles within an alternating magnetic field are consequences of several types of loss processes, including hysteresis and Néel and Brownian relaxation.[34–36] As the magnitude of magnetically induced heat changes strongly depends on particle size, comparable heating rates of the two colloid populations suggest only minimum changes in particle size due to surface immobilization of a phospholipid layer. This conclusion is consistent with TEM data shown in Fig. 2(c).

Therapeutically desired hyperthermia conditions ($> 40°C$) were achieved within 10–15 min using both control and phospholipid-modified Fe_3O_4 nanoparticles. DSC analysis indentified a T_m of 39.7°C for the lipid layer immobilized on Fe_3O_4 nanoparticles (Fig. 4). It is, therefore, anticipated that hyperthermia-induced release of colloid-associated payload from these phospolipid-modified colloids will require exposure to an alternating magnetic field of similar strength as used in this simple *in vitro* experiment for at least 10 min. If more rapid release profiles are desired, smaller Fe_3O_4 nanoparticles could be used due to the exponential relationship between Néel relaxation time and particle volume.[37]

3.4. *Loading and thermoresponsive release of dansylcadaverine*

Phospholipid bilayers immobilized on the surface of superparamagnetic nanoparticles are predicted to serve as carriers for predominantly lipophilic guest molecules that are stabilized within the hydrophobic fatty acid tails of the phospholipids. In contrast to liposomes, which contain a hydrophilic core suitable for encapsulation of hydrophilic guest molecules,[38,39] the geometry of surface-immobilized phospholipid bilayers does not allow sequestering of a significant water volume between colloid surface and phospholipid head groups.[40] To determine the loading capacity of phospholipid-modified Fe_3O_4 nanoparticles, the lipophilic dye dansylcadaverine was used as drug surrogate. The amount of colloid-associated dye was quantified by fluorescence spectroscopy following dissolution of lipid layer in methanol. On average, 479 ± 124 ng of dansylcadaverine were recovered per mg of Fe_3O_4 nanoparticles from different fabrication batches ($n = 10$). Future experiments using therapeutically effective drugs will reveal whether the loading capacity of phospholipid-modified Fe_3O_4 nanoparticles will be sufficient to prepare clinically required doses. Currently, FDA-approved formulations of superparamagnetic Fe_3O_4 nanoparticles used as MRI contrast agents, including Endorem® and Resovist®, are administered in doses between 50–100 mg Fe_3O_4.

To assess thermoresponsive release properties of phospholipid-modified Fe_3O_4 nanoparticles *in vitro*, dye-loaded colloid suspensions prepared in PBS were exposed for 60 min to 25°C and 70°C using a temperature-controlled water bath. Dansylcadaverine concentrations released from the carrier were quantified after magnetic separation by fluorescence spectroscopy. At 25°C, which is below the experimentally determined T_m of the colloid-immobilized lipid layer, 8.4 ± 1.7% ($n = 4$) of the loaded dye was recovered in the dissolution media after 1 h. In contrast, release rate at 70°C was significantly greater reaching on average 23.4 ± 6.8% ($n = 4$). This corresponds to approximately 106 ng of dansylcadaverine released per mg of Fe_3O_4 nanoparticles. Similar to conventional thermoresponsive drug delivery systems such as liposomes or polymeric nanoparticles, release of encapsulated payload occurs even at temperature below T_m. Considering the hydrophobic properties of dansylcadaverine, we speculated that bilayer imperfections and/or dye associated with the phospholipid surface contribute to these results. Most importantly, however, our data underline that increased mobility of phospholipids at a temperature greater than T_m translates into accelerated payload release. Time-dependent

release profiles in the presence of magnetically induced hyperthermia will facilitate delineating kinetic aspects of this thermoresponsive payload release from phospholipid-modified Fe_3O_4 nanoparticles in greater detail.

4. Conclusion

The results from this study demonstrate for the first time successful immobilization of a phospholipid assembly on the surface of superparamagnetic nanoparticles via high-affinity avidin−biotin interactions. Physicochemical and morphological evaluations revealed deposition of a 2−3 nm layer of DPPC/DSPE-PEG2000-biotin (95:5) on avidin-coated Fe_3O_4 nanoparticles with a gel/liquid-crystalline phase transition temperature of 39.7°C. The zeta potential of Fe_3O_4 colloids in PBS decreased from −23.6 to −5.0 mV as a consequence of phospholipid immobilization. Nevertheless, the heating properties of these superparamagnetic nanoparticles exposed to an alternating magnetic field were not significantly affected. Hyperthermia-relevant temperatures > 40°C were achieved within 10−15 min using a 7-mT magnetic field alternating at a frequency of 1 MHz. Loading of the surface-associated phospholipid layer with the hydrophobic dye dansylcadaverine was accomplished at an efficiency of 479 ng/mg Fe_3O_4. Release of this drug surrogate was significantly dependent on temperature. On average, release rate of this dye was 2.5-fold greater when nanoparticles were exposed to a temperature above the T_m of the colloid-associated lipid layer.

These data underline the feasibility of preparing novel, stimulus-induced drug delivery systems, where payload release from a colloid-immobilized phospholipid assembly is triggered by hyperthermia in response to an alternative magnetic field. In contrast to previously described thermoresponsive polymers, including analogs of poly(*N*-substituted acrylamide) and poly(ethylene glycol), deposition of a phospholipid lipid layer on the surface of superparamagnetic nanoparticles offers the opportunity to incorporate a multitude of lipid-based targeting ligands and hydrophilic shielding groups using conventional technology that has been established for liposomal drug carriers. This may significantly accelerate clinical translation of phospholipid-modified superparamagnetic nanoparticles as alternative drug delivery systems to improve inadequate response to conventional therapeutic regimens.

Acknowledgments

This work was supported in part by a tuition scholarship from the National Science Foundation (EEC 0939320 to Ch. H.) and grants from the National Institutes of Health (HD-48512 to G.M.P.) and the Argonne National Laboratory/Department of Energy (No. 97-30461 to D.S.). The authors are grateful to Dr. Necati Kaval (Department of Chemistry, University of Cincinnati) for his assistance with DSC and ATR-FTIR experiments.

References

1. S. L. Huang, *Adv. Drug Deliv. Rev.* **60**, 1167 (2008).
2. M. Ishitobi, E. Shin and N. Kikkawa, *Int. J. Clin. Oncol.* **6**, 55 (2001).
3. W. G. Pitt, G. A. Husseini and B. J. Staples, *Expert. Opin. Drug Deliv.* **1**, 37 (2004).
4. M. Schmitt-Sody, S. Strieth, S. Krasnici, B. Sauer, B. Schulze, M. Teifel, U. Michaelis, K. Naujoks and M. Dellian, *Clin. Cancer Res.* **9**, 2335 (2003).
5. Y. Shamay, L. Adar, G. Ashkenasy and A. David, *Biomaterials* **32**, 1377 (2011).
6. C. M. Spencer and D. Faulds, *Drugs* **48**, 794 (1994).
7. M. Bikram, A. M. Gobin, R. E. Whitmire and J. L. West, *J. Control. Release* **123**, 219 (2007).
8. B. B. Youan, *J. Control. Release* **98**, 337 (2004).
9. D. E. Thurston, *Chemistry and Pharmacology of Anticancer Drugs*, Chapter 7 (CRC Press, Boca Raton, 2007), pp. 157−192.
10. C. Y. Gong, P. W. Dong, S. Shi, S. Z. Fu, J. L. Yang, G. Guo, X. Zhao, Y. Q. Wei and Z. Y. Qian, *J. Pharm. Sci.* **98**, 3707 (2009).
11. D. R. Khan, E. M. Rezler, J. Lauer-Fields and G. B. Fields, *Chem. Biol. Drug Des.* **71**, 3 (2008).
12. P. Pradhan, J. Giri, F. Rieken, C. Koch, O. Mykhaylyk, M. Doblinger, R. Banerjee, D. Bahadur and C. Plank, *J. Control. Release* **142**, 108 (2010).
13. S. Purushotham and R. V. Ramanujan, *Acta Biomater.* **6**, 502 (2010).
14. H. B. Na, I. C. Song and T. Hyeon, *Adv. Mater.* **21**, 2133 (2009).
15. C. Alexiou, R. J. Schmid, R. Jurgons, M. Kremer, G. Wanner, C. Bergemann, E. Huenges, T. Nawroth, W. Arnold and F. G. Parak, *Eur. Biophys. J.* **35**, 446 (2006).
16. A. S. Lubbe, C. Alexiou and C. Bergemann, *J. Surg. Res.* **95**, 200 (2001).
17. S. Balivada, R. S. Rachakatla, H. Wang, T. N. Samarakoon, R. K. Dani, M. Pyle, F. O. Kroh, B. Walker, X. Leaym, O. B. Koper, M. Tamura, V. Chikan, S. H. Bossmann and D. L. Troyer, *BMC Cancer* **10**, 119 (2010).

18. V. S. Narang, G. M. Pauletti, P. W. Gout, D. J. Buckley and A. R. Buckley, *Chemotherapy* **53**, 210 (2007).
19. H. Xu, L. Cui, N. Tong and H. Gu, *J. Am. Chem. Soc.* **128**, 15582 (2006).
20. G. Gopalakrishnan, I. Rouiller, D. R. Colman and R. B. Lennox, *Langmuir* **25**, 5455 (2009).
21. A. L. Troutier and C. Ladaviere, *Adv. Coll. Interf. Sci.* **133**, 1 (2007).
22. H. T. Wiogo, M. Lim, V. Bulmus, J. Yun and R. Amal, *Langmuir* **27**, 843 (2011).
23. N. Kucerka, S. Tristram-Nagle and J. F. Nagle, *Biophys. J.* **90**, L83 (2006).
24. J. Repakova, J. M. Holopainen, M. R. Morrow, M. C. McDonald, P. Capkova and I. Vattulainen, *Biophys. J.* **88**, 3398 (2005).
25. Y. Chen and G. D. Bothun, *Langmuir* **25**, 4875 (2009).
26. D. A. Mannock, R. N. Lewis and R. N. McElhaney, *Biophys. J.* **91**, 3327 (2006).
27. M. Kastantin, B. Ananthanarayanan, P. Karmali, E. Ruoslahti and M. Tirrell, *Langmuir* **25**, 7279 (2009).
28. C. Naumann, T. Brumm and T. M. Bayerl, *Biophys. J.* **63**, 1314 (1992).
29. T. Brumm, K. Jorgensen, O. G. Mouritsen and T. M. Bayerl, *Biophys. J.* **70**, 1373 (1996).
30. E. Okamura, J. Umemura and T. Takenaka, *Vib. Spectrosc.* **2**, 95 (1991).
31. M. Cagnasso, V. Boero, M. A. Franchini and J. Chorover, *Coll. Surf. B Biointerf.* **76**, 456 (2010).
32. M. Mahmoudi, A. Simchi, M. Imani, M. A. Shokrgozar, A. S. Milani, U. O. Hafeli and P. Stroeve, *Coll. Surf. B Biointerf.* **75**, 300 (2010).
33. Y. Park, R. Huang, D. S. Corti and E. I. Franses, *J. Coll. Interf. Sci.* **342**, 300 (2010).
34. R. Hergt, S. Dutz, R. Muller and M. Zeisberger, *J. Phys.-Condens. Mat.* **18**, S2919 (2006).
35. Z. X. Li, M. Kawashita, N. Araki, M. Mitsumori, M. Hiraoka and M. Doi, *Mater. Sci. Eng. C-Mater.* **30**, 990 (2010).
36. P. P. Vaishnava, R. Tackett, A. Dixit, C. Sudakar, R. Naik and G. Lawes, *J. Appl. Phys.* **102** (2007).
37. R. E. Rosensweig, *J. Magn. Magn. Mater.* **252**, 370 (2002).
38. M. Hossann, M. Wiggenhorn, A. Schwerdt, K. Wachholz, N. Teichert, H. Eibl, R. D. Issels and L. H. Lindner, *Biochim. Biophys. Acta-Biomembranes* **1768**, 2491 (2007).
39. K. Iga, N. Hamaguchi, Y. Igari, Y. Ogawa, H. Toguchi and T. Shimamoto, *Int. J. Pharm.* **57**, 241 (1989).
40. R. Tero, H. Watanabe and T. Urisu, *Phys. Chem. Chem. Phys.* **8**, 3885 (2006).